Research Article

The thresholding problem and variability in the EEG graph network parameters

Timofey Adamovich*[a, b], Ilya Zakharov[a, b], Anna Tabueva[a, b], Sergey Malykh[a, b]
[a] Psychological Institute of Russian Academy of Education, Moscow, Russia
[b] Ural Federal University named after the first President of Russia B.N. Yeltsin, Yekaterinburg, Russia

*Corresponding author. E-mail address: tadamovich11@gmail.com

Keywords: resting-state EEG, thresholding, functional connectivity, graph analysis, network analysis

Abstract

The graph thresholding is a frequently used practice of eliminating the weak connections in brain functional connectivity graphs. The main aim of the procedure is to delete the spurious connections in the data. However, the choice of the threshold is arbitrary and the effect of the threshold choice in not fully understood. Here we present the description of the changes in the global measures of a functional connectivity graph depending on the different proportional thresholds based on the 146 resting-state EEG recordings. The dynamics is presented in five different synchronization measures (wPLI, ImCoh, Coherence, ciPLV, PPC) in sensors and source spaces. The analysis shows significant changes in the graph's global connectivity measures as a function of the chosen threshold which may influence on the outcome of the study. The choice of the threshold could lead to the different study conclusions, thus it is necessary to improve the reasoning behind the choice of the different analytic options and consider adoption of different analytic approaches.

Introduction

Brain connectomics is a rapidly developing field of study investigating the interactions between relatively homogeneous brain cell circuits (or brain areas). In response to the external environment, the various areas across the cortex begin to interact, forming a macroscale whole-brain network (Sadaghiani et al., 2022). One way to understand this network comes from mathematical graph theory which can describe complex structures and dynamics within networks (Avena-Koenigsberger et al., 2018). The network approach is based on a pairwise matrix of connections between nodes and was used in various studies, to examine the relations between brain characteristics of brain networks with different psychological phenomena, such as cognitive processes, personality or psychopathology (Beaty et al., 2018; Finn et al., 2015; Markett et al., 2018; Smith et al., 2018; Toschi et al., 2018; van den Heuvel & Sporns, 2019) based on fMRI or DTI (Buckner et al., 2013; Liégeois et al., 2017; Stevens & Spreng, 2014), EEG/MEEG and fNIRS (Allen et al., 2018; van Diessen et al., 2015). data.

Network neuroscience is a new and developing area, and one of its challenges is considerable variability in the connectivity calculation routines, which is not always detailed and explicitly motivated in studies. Estimation of the functional connections graph via various indexes (see (Bastos & Schoffelen, 2016) for a review) creates a full adjacency matrix that makes no sense anatomically or mathematically. The next step is usually the creation of the sparse matrix by choosing some threshold value as a cut-off point below which the values are removed (Rubinov & Sporns, 2010). However, while thresholding is a good way to reduce the possibility of too much influence of spurious or weak connections, it leads to confounds related to the arbitrary choice of the calculation routines.

There is no consensus in the scientific society as to how to choose the specified thresholds. There are two main ways to estimate the threshold value. Absolute threshold is a specific value below which the connection is considered as spurious and proportional threshold leaves the percent of connections in the matrix. Another issue is the selection of the value and, thus, the number of edges in the resulting network.

The thresholding procedure has been criticized in numerous studies, both from theoretical and practical positions (Avena-Koenigsberger et al., 2018). The choice of the threshold could lead to incomparable results (Garrison et al., 2015, van Wijk et al., 2010). In a recent fMRI study, the range of absolute thresholds varied from 0.1 to 0.8 correlation coefficient and proportional thresholds from 2 to 40% lead the graphs to be incomparable (Buchanan et al., 2020; Civier et al., 2019). The fMRI graph-based connectivity metrics are unstable across various threshold values (and overall, more stable across proportional thresholds compared to absolute, (Garrison et al., 2015). In a recent DTI study (Diffusion Tensor Tomography, Civier et al., 2019) the thresholding procedure has been shown to lead to differences in connectivity metrics if more than 70% of the connections between the nodes were removed. Also, it has been shown that calculating the connectivity metrics without thresholding is feasible and, thus, there is now no practical utility in this step of the analysis for DTI data.

While the thresholding procedure is widely used, there is also another, data-driven way to prepare brain data for network analysis, which is based on algorithmic reduction of the number of nodes. The most popular algorithms are based on the spanning tree procedure (e.g. minimum or condensed spanning tree MST or CST, respectively), which constructs a unique and acyclic sub-network with a fixed number of connections (see, for example, (Dimitriadis et

al., 2017; Dimitriadis, López, et al., 2018; Dimitriadis, Routley, et al., 2018). In the brain imaging data, the spanning-tree approach could be very useful, but a direct comparison of the results obtained with thresholding approaches and various data-driven approaches is needed.

Initially, connectivity studies were mostly based on various types of MRI (both structural and functional) data. However, a considerable part of brain activity cannot be captured by MRI due to its poor temporal resolution. The M/EEG allows the analysis of quick or high-frequency oscillations (Bastos et al., 2015; Fries, 2015) and reflect the efficiency of communication between brain areas (Palva & Palva, 2011; Stam & van Straaten, 2012, Fries, 2015) But, according to the recent International Federation of Clinical Neurophysiology (IFCN) report, for M/EEG studies "there is no clear consensus on the statistical thresholds for the confirmation of a significant effect at the scalp or source-level" (Babiloni et al., 2020). As far as we know the effect of the thresholding for the calculation of the EEG-derived connectivity graph metrics has never been directly assessed.

The article is based on a study first reported in the Journal of Physics: Conference Series (Zakharov et al., 2021) and presents the extended analysis.

Results

The distribution of the connectivity strength

The connectivity graphs could be influenced by the individual differences in connectivity strength. Here we illustrate the descriptive statistics of individual connectivity strength distributions. The plots are presented for each connectivity measure in the sensor (left column) and source (right column) space. From top to bottom: Median, Mean, Median Absolute Deviation, SD.

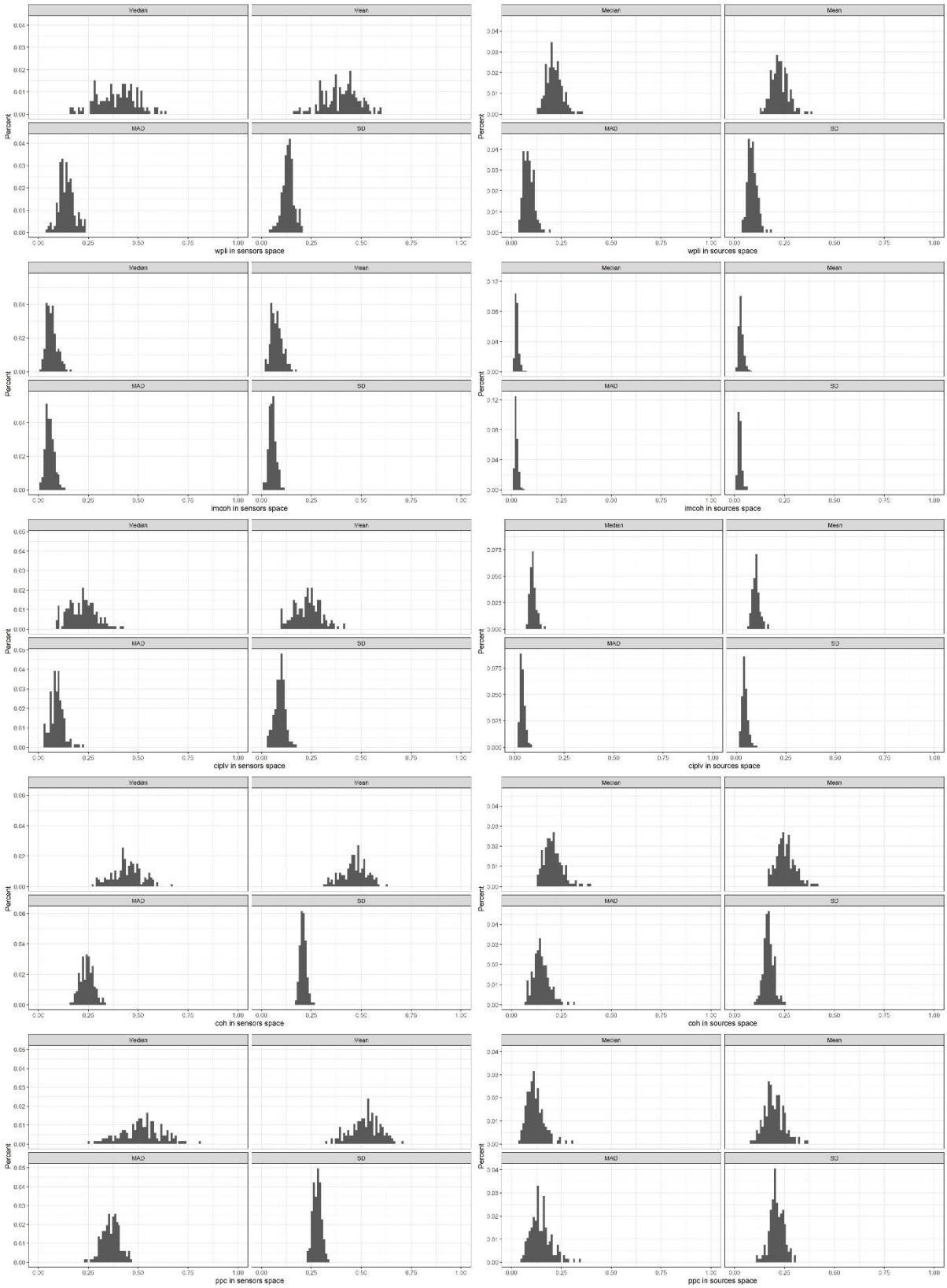

Figure 1. *Distribution of descriptives for connectivity measures in sensor and source space*

The shape of the distribution of the mean and standard deviation in the sample point out the variability of absolute values and fluctuations in the shape in the individual connectivity strength distributions. The differences in the absolute connectivity strength could impact the graph measures (mostly connection-weight based, e.g. path length, (van Wijk et al., 2010), however, structural properties of the graph should remain the same. For the thresholds that lead to low graph densities the problem of a disconnected graph might appear which will lead to the inability to estimate the path length and clustering coefficient of the overall network.

To overcome the disconnected graphs problem the procedure of eliminating the isolated nodes from the graph is often used. Isolated nodes almost inevitably appear with high thresholds, thus leading to the differences in the number of nodes in the graphs which could lead to biased results. According to our data (see Appendix) the number of isolated nodes increases with higher threshold level to the point where there is no matrix without a disconnected node. It is possible that on the higher thresholds graph measures are derived from the graph with different sets of nodes. Thorough discussion of the missing nodes is beyond the scope of the paper.

Threshold-level induced changes in the graph measures

In the next step of our analysis to investigate the effect of the thresholding values on the chosen graph metrics we trace the changes in the graph measures retrieved from the different chosen thresholds. The results are presented in figures 2-3.

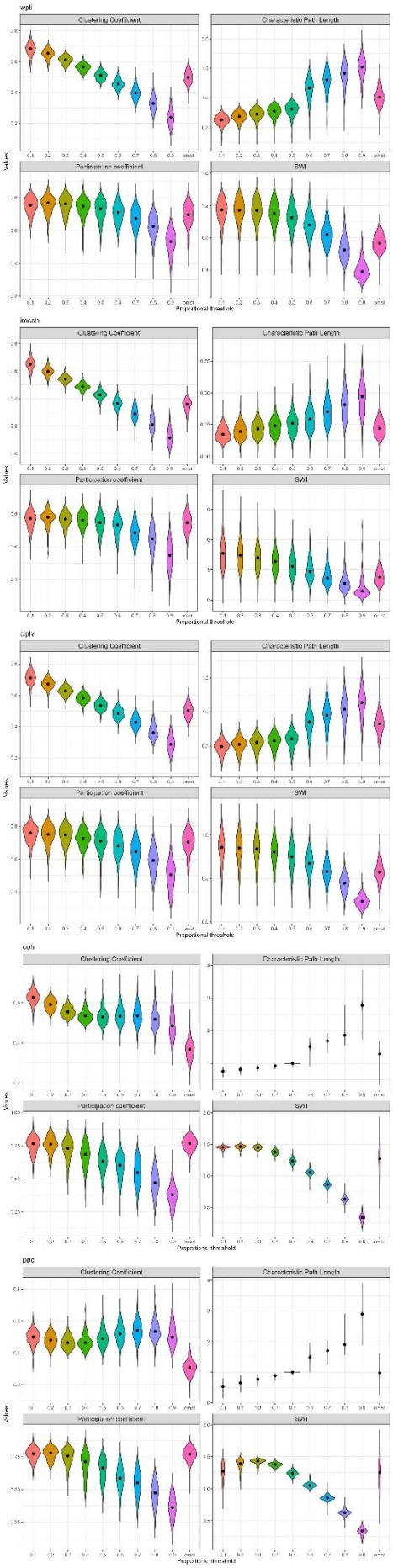
wpli
Clustering Coefficient
Characteristic Path Length
Participation coefficient
SWI
Values
Proportional threshold
imcoh
Clustering Coefficient
Characteristic Path Length
Participation coefficient
SWI
Values
Proportional threshold
ciplv
Clustering Coefficient
Characteristic Path Length
Participation coefficient
SWI
Values
Proportional threshold
coh
Clustering Coefficient
Characteristic Path Length
Participation coefficient
SWI
Values
Proportional threshold
ppc
Clustering Coefficient
Characteristic Path Length
Participation coefficient
SWI
Values
Proportional threshold

Figure 2. *Effect of density thresholding on graph measures in sensor space***.** Five measures are presented in the following order (top-to-bottom): wPLI, imcoh, ciPLV, coherence, PPC On each plot four measures are presented (left-to-right, top-to-bottom): Clustering Coefficient, Characteristic PL, Participation Coefficient, SWI. The utmost X-axis value on the right is a value obtained via the OMST method.

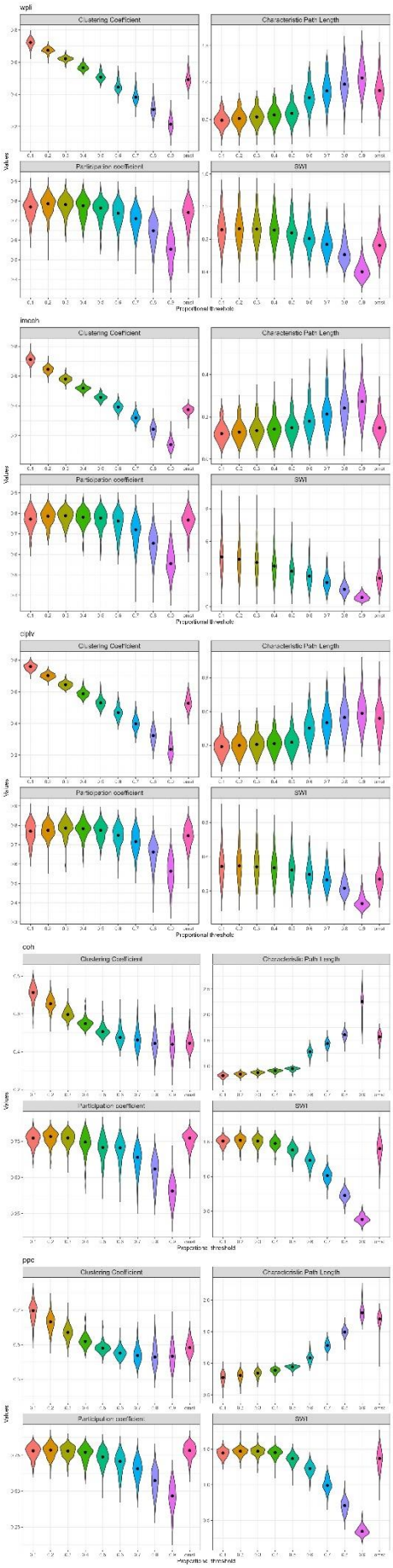
wpli
Clustering Coefficient
Characteristic Path Length
Participation coefficient
SWI
Values
Proportional threshold
imcoh
Clustering Coefficient
Characteristic Path Length
Participation coefficient
SWI
Values
Proportional threshold
ciplv
Clustering Coefficient
Characteristic Path Length
Participation coefficient
SWI
Values
Proportional threshold
coh
Clustering Coefficient
Characteristic Path Length
Participation coefficient
SWI
Values
Proportional threshold
ppc
Clustering Coefficient
Characteristic Path Length
Participation coefficient
SWI
Values
Proportional threshold

Figure 3. *Effect of density thresholding on graph measures in source space.* Five measures are presented in the following order (left-to-right, top-to-bottom): wPLI, imcoh, ciPLV, coherence, PPC. On each plot, four measures are presented (left-to-right, top-to-bottom): Clustering Coefficient, Characteristic PL, Participation Coefficient, SWI. The utmost X-axis value on the right is the value obtained via OMST, second rightmost - via AUC.

Characteristic Path length increases with the decreasing density, Clustering coefficient, Participation coefficient and SWI decreases with decreasing density. Also, there are differences in the variance on the different thresholds with higher variance on the higher thresholds. The dynamics of the differences are similar in all synchronization measures and both spaces.

Linear regression analysis of the threshold-level induced dynamics

At the next step of our analysis, we wanted to estimate the proportion of the variance in the calculation of graph metrics as the result of the thresholding procedure. Linear regression analysis was performed to investigate the dependence of measures from the thresholding value. All coefficients are significant ($p<0.05$)

Table 1. Linear regression of the brain connectivity measures.

	Sensor Space			Source Space		
	Intercept	Density value (Coef)	Adj.R.Squared	Intercept	Density value (Coef)	Adj.R.Squared
	wPLI					
Characteristic PL	0.39	1.19	0.76	0.32	0.78	0.62

Clustering Coefficient	0.76	-0.54	0.91	0.8	-0.61	0.95
SWI	1.34	-0.81	0.56	1.07	-0.55	0.39
Participation coefficient	0.81	-0.25	0.44	0.83	-0.23	0.45
			imcoh			
Characteristic PL	0.11	0.345	0.48	0.08	0.18	0.37
Clustering Coefficient	0.73	-0.64	0.93	0.78	-0.68	0.97
SWI	5.4	-4.3	0.46	5.5	-4.78	0.53
Participation coefficient	0.83	-0.23	0.43	0.84	-0.22	0.46
			ciPLV			
Characteristic PL	0.3	0.85	0.61	0.2	0.41	0.49

Clustering Coefficient	0.77	-0.51	0.91	0.83	-0.63	0.95
SWI	1	-0.68	0.53	0.61	-0.35	0.36
Participation coefficient	0.81	-0.28	0.49	0.83	-0.22	0.43
			Coherence			
Characteristic PL	0.24	2.2	0.81	0.44	1.52	0.78
Clustering Coefficient	0.61	-0.12	0.33	0.71	-0.34	0.77
SWI	1.79	-1.4	0.87	1.85	-1.32	0.79
Participation coefficient	0.84	-0.47	0.65	0.87	-0.41	0.59
			PPC			
Characteristic PL	0	2.6	0.84	0.49	1.2	0.83

Clustering Coefficient	0.46	0.07	0.1	0.68	-0.32	0.69
SWI	1.67	-1.22	0.75	1.8	-1.29	0.76
Participation coefficient	0.87	-0.5	0.69	0.87	-0.36	0.6

There is a substantial linear trend in the dynamic of the measure changes, as reflected in the R-squared values. The R-squared ranges from 0.1 to 0.97 with a median value of 0.62. R-squared also varies in the different measures and spaces. Although there is a strong linear component in the measure's dynamics, most of them show a more complex pattern of changes. At low thresholds, the changes are smaller than at the high thresholds. The clustering coefficient demonstrates an even more peculiar pattern of changes in some cases, it has a plateau in the middle thresholds.

Correlational analysis of measures on the different thresholds

Correlations between the different thresholds were used to identify the relations between the different thresholds. In the following plots, we present the correlations between measures on different thresholds. On the top half, sensor-space correlations are presented, on the lower - source-space. Only significant correlations ($p>0.05$) are presented.

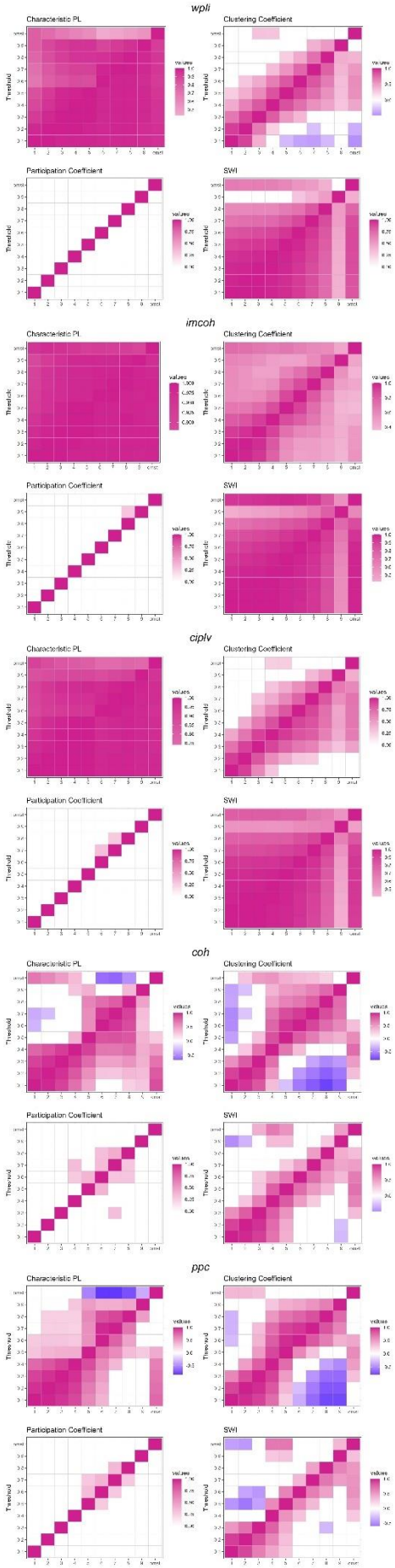
wpli
Characteristic PL
Clustering Coefficient
Participation Coefficient
SWI
imcoh
Characteristic PL
Clustering Coefficient
Participation Coefficient
SWI
ciplv
Characteristic PL
Clustering Coefficient
Participation Coefficient
SWI
coh
Characteristic PL
Clustering Coefficient
Participation Coefficient
SWI
ppc
Characteristic PL
Clustering Coefficient
Participation Coefficient
SWI
Threshold
values

Figure 4. *Correlation of graph measures on different thresholds***.** Five measures are presented in the following order (left-to-right, top-to-bottom): wPLI, imcoh, ciPLV, coherence, PPC. On each plot four measures are presented (left-to-right, top-to-bottom): Clustering Coefficient, Characteristic PL, Participation Coefficient, SWI. The utmost X-axis value on the right is the value obtained via OMST.

The differences in the correlational structure between different thresholds could reveal the linearity and non-linearity in the intra-threshold changes. The highly correlated structure would indicate relative consistency in the network structure across different thresholds, while uncorrelated structure shows instability in the network structure.

A few points could be derived from our results. First, there are differences in the correlation structure between the different synchronization measures - there are two distinct groups wPLI and ciPLV and imcoh, coherence and PPC with distinct patterns of correlational structure. Second, Characteristic Path length and clustering coefficient are relatively correlated in neighbouring thresholds in all measures. Third, the participation coefficient is not intercorrelated. Overall, these results could show the substantial inconsistency in the network structure that could indicate the incongruity between global and local network measures

Structure of the functional connectivity graphs on the different thresholds

As the final step in the analysis, to understand the graphs behind the measures, we decided to trace changes in the structure of the functional connectivity graphs via the edge probability graphs.

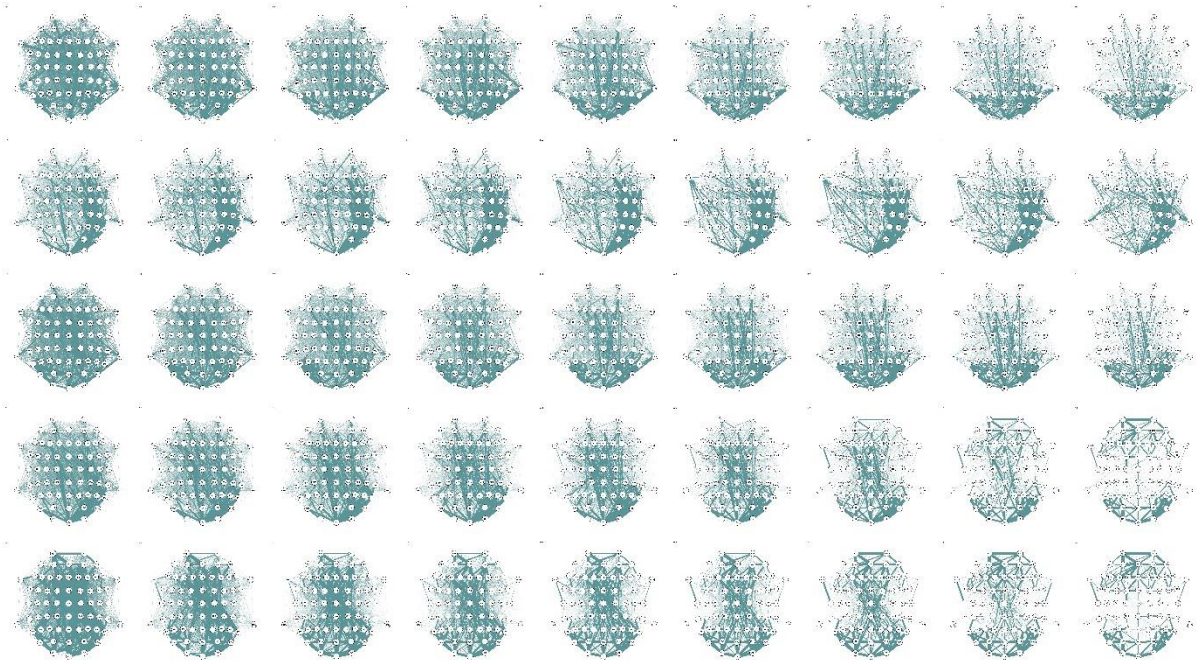

Figure 5. *Edge probability graphs across different thresholds in sensor space.* The thickness of the edge reflects the probability. The edge weights were scaled to the range [0, 1] across all thresholds. From top to bottom: wPLI, imcoh, ciPLV, Coherence, PPC

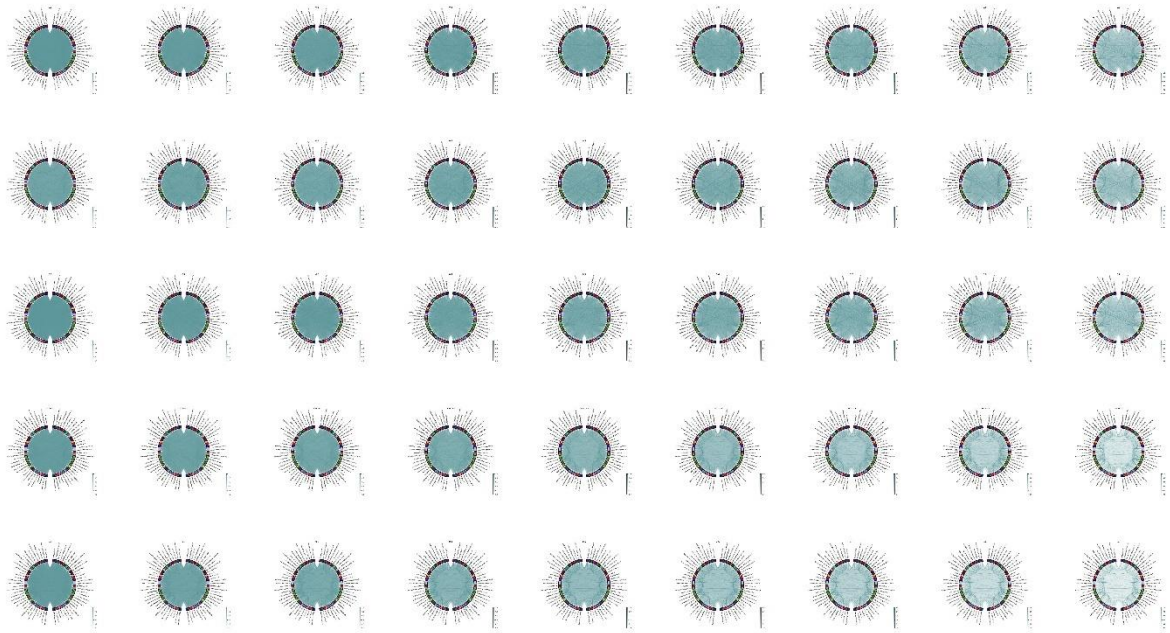

***Figure 6**. Edge probability graphs across different thresholds in source space.* The thickness of the edge reflects the probability. The edge weights were scaled to the range [0, 1] across all thresholds

The edge probability graphs reflect the strongest connections in the connectivity matrices and the stability of connectivity estimation in the sample. If the edge is strong and stable across the sample, the probability of the node existence tends to be 1. The plots show that strong connections show up more clearly on the higher thresholds.

Comparison of traditional thresholding approach and data-driven techniques

To avoid the arbitrarily chosen thresholds the data-driven approaches have been developed. We chose the orthogonal MST method (Dimitriadis et al., 2017) to represent the data-driven techniques as it is believed that this method creates denser and potentially more meaningful networks. The direct comparison of the networks requires the same density in both networks. The mean density of the OMST-derived graph is 0.45+0.01, which is equivalents to the 0.55 quantile threshold. The following comparison is performed between OMST-derived and 0.55 quantile graphs.

Table 2. T-statistic comparison between OMST-graph and thresholded graph of similar density

	Sensors space			Source space		
	t-stat	p-value	Cohen's d	t-stat	p-value	Cohen's d
	wPLI					
CPL	174,41	0,02	0,26	121,87	0,00	-1,10

Clustering Coefficient	80,24	0,00	-0,43	79,91	0,00	-0,49
SWI	166,54	0,00	2,02	141,97	0,00	0,81
Participation Index	119,57	0,00	0,44	124,86	0,00	0,33
			imcoh			
CPL	44,60	0,00	0,57	27,44	0,10	0,18
Clustering Coefficient	65,26	0,00	1,13	70,65	0,00	2,46
SWI	541,81	0,00	0,90	516,62	0,00	0,48
Participation Index	121,35	0,06	-0,20	125,87	0,48	-0,08
			Coherence			
CPL	236,67	0,00	1,29	194,48	0,00	-4,52

Clustering Coefficient	88,93	0,00	3,78	82,48	0,00	1,23
SWI	190,56	0,00	-0,73	217,19	0,00	-0,67
Participation Index	100,09	0,00	-2,12	115,42	0,00	-0,93
			PPC			
CPL	224,03	0,00	2,06	163,13	0,00	-8,16
Clustering Coefficient	84,33	0,00	3,81	77,57	0,00	-0,45
SWI	190,77	0,00	-0,54	215,81	0,00	-0,59
Participation Index	102,07	0,00	-1,89	117,62	0,00	-1,21
			ciPLV			
CPL	126,52	0,00	-0,37	69,75	0,00	-1,03

Clustering Coefficient	84,72	0,01	0,29	83,03	0,00	-0,84
SWI	117,54	0,00	0,98	78,55	0,00	0,67
Participation Index	116,14	0,89	0,01	125,55	0,02	0,26

The results of comparison between OMST and thresholded graphs show substantial differences between the two. The direction of the changes is ambiguous and unstable across different synchronization measures both in sensor and source spaces, e.g. OMST CPL is lower in PPC - sensor networks and higher in the ciPLV-sensor networks. This might indicate the influence of the individual synchronization strength distribution on the estimation of orthogonal MSTs.

epi OMST

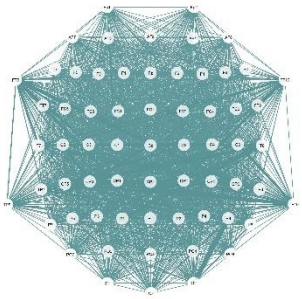

epi Traditional threshold

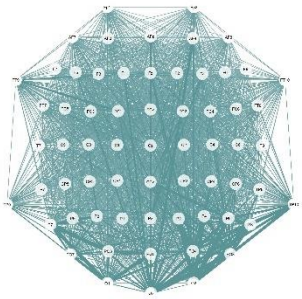

inrcoh OMST

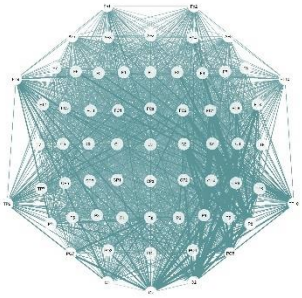

inrcoh Traditional threshold

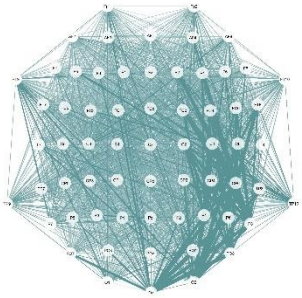

cpy OMST

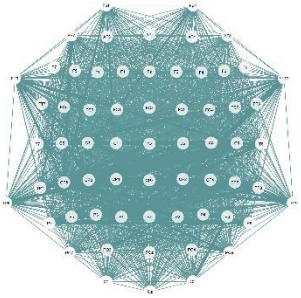

cpy Traditional threshold

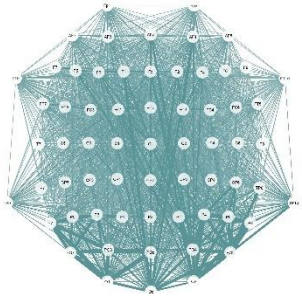

coh OMST

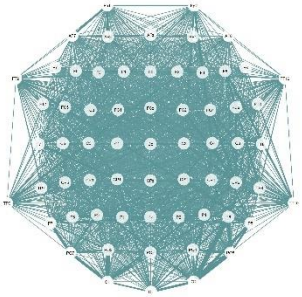

coh Traditional threshold

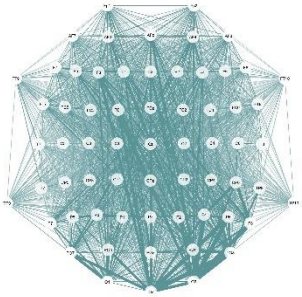

ppc OMST

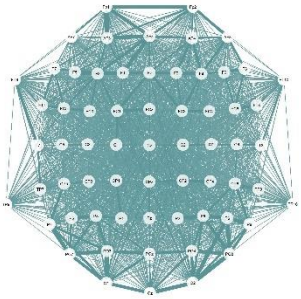

ppc Traditional threshold

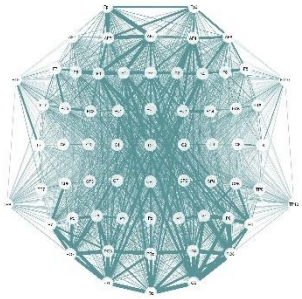

Figure 7. *Graph structure for OMST-derived graphs and thresholded graphs of equal density in sensor space.* The left graph in a row is OMST-derived, right - thresholded. Synchronization measures by row: wpli, imcoh, ciplv, coh, ppc.

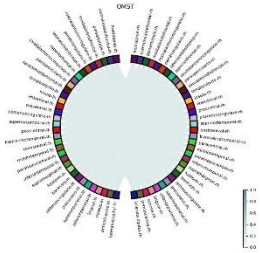
OMST

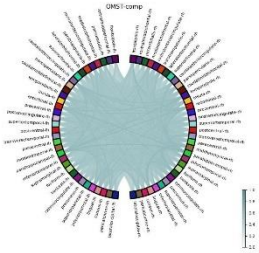
OMST-comp

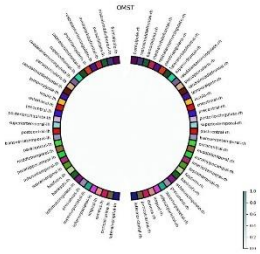
OMST

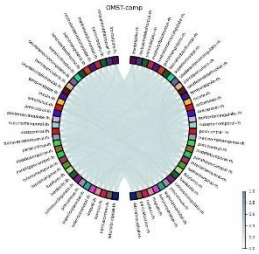
OMST-comp

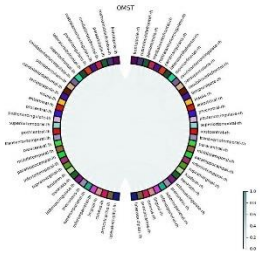
OMST

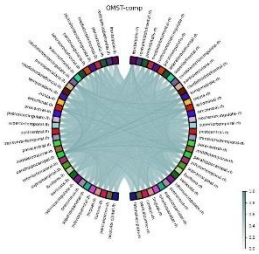
OMST-comp

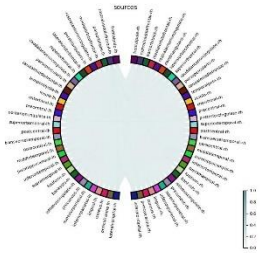
sources

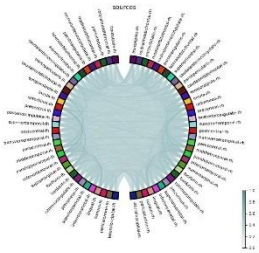
sources

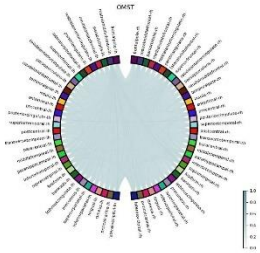
OMST

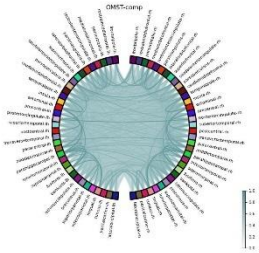
OMST-comp

Figure 8. *Graph structure for OMST-derived graphs and thresholded graphs of equal density in source space*. The left graph in a row is OMST-derived, right - thresholded. Right circles indicate areas of the left hemisphere, blue - areas of the right hemisphere. Synchronization measures by row: wpli, imcoh, ciplv, coh, PPC

In the source space, there is a difference between the edge probability in the OMST-graphs and thresholded graphs. This might reflect individual differences in the graphs. The probability of the edge existence in the OMST-graphs is lower than in the traditional approach and might indicate the MST algorithm being more prone to the individual connectivity strength distribution.

Gender differences on different thresholds

The main aim of the functional connectivity studies is to estimate the specificity of brain networks in different conditions, such as gender, different level of intelligence or specific task. However, the chosen thresholds could affect the characteristics of the groups, leading to the absence or the presence of the effect of interest depending on the thresholding value. The subjective choice of thresholds results in differences in the absolute values of graph metrics at different levels, values, but these differences will not necessarily be reflected in the experimental results. Here we use the genders differences to model the effect of the thresholding procedure on the group comparisons.

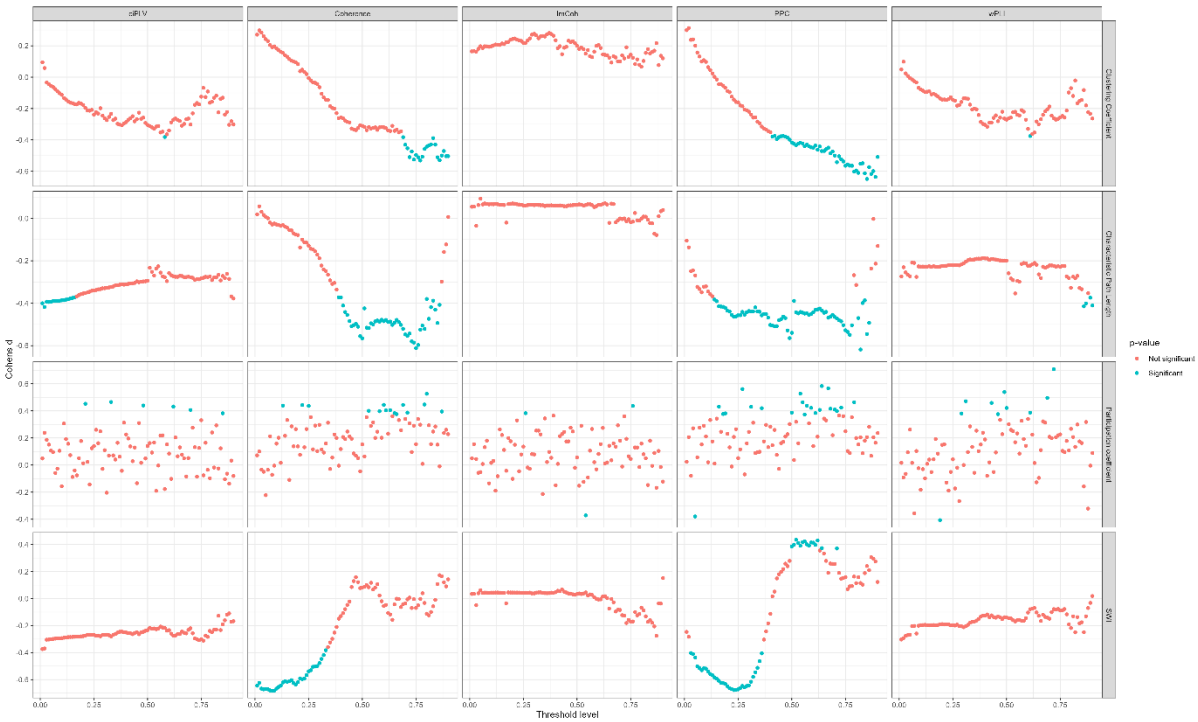

Figure 9. The Cohen's d of the gender comparison on the different thresholds in sensor space. Permutation t-test was used to estimate the differences between two groups. The red dots represents the effect as significant (p-value < 0.05), the blue represents the non-significant effect (p-value> 0.05)

Figure 10. The Cohen's d of the gender comparison on the different thresholds in source space. Permutation t-test was used to estimate the differences between two groups. The red dots represents the effect as significant (p-value < 0.05), the blue represents the non-significant effect (p-value> 0.05)

Our analysis suggests that the results of the group comparisons might differ depending on the threshold level. For example, fo r the participation coefficient gender differences are non-significant for the majority of the thresholds, but not all of them. It is important to note that those thresholds are scattered across the threshold levels. For other metrics there are monotonic changes in the magnitude of the group differences with the "significant" intervals. These intervals, however, can start far below the most widely used thresholds, located around 0.8 threshold. In contrast, at high levels of the thresholds there is variability in the effect size, which indicates considerable instability in the estimation of group differences. There are also intervals of the significant differences on the lower thresholds (around the 0.25 threshold), indicating the possible group differences specifically for the weak connections. Fourth, in our data a peculiar case occurs, the SWI for the PPC in sensor space has two significant intervals with the opposite Cohen's d values. At low thresholds the males have higher values of SWI than females, while at high thresholds the effect was the opposite. In this case, the choice of threshold determines not only the conclusion about the presence or absence of an effect, but also about its direction.

Discussion

The present article aimed to analyze the effect of the thresholding procedure on graph construction from EEG resting state data. According to our results, the thresholding procedure leads to substantial variability in the data. Overall, we have found that:

1. Global graph metrics vary as a function of density level.

2. Density-related graph measures (characteristic path length, clustering coefficient, participation coefficient and SWI) dynamic have a substantial linear component.

3. Proportional thresholding led to substantial distortions in the graph structure, indicated by the structure of correlations between different thresholds.

4. Data-driven algorithms may give significantly different results from the traditional thresholding procedure of corresponding density.

5. The chosen threshold may influence on the outcome of the analysis (e.g., presence or absence of the effect of group comparisons).

These discrepancies between the network structure and graph-based metrics on different thresholds are extremely important in light of the widely discussed reproducibility crisis in modern science making it hard to estimate the comparability of the results performed with different analysis pipelines. Overall, according to our results, the way the researcher solves the thresholding issue heavily affects the outcome of the connectivity analysis. Our results add to the previous results by Garrison and colleagues (2015) (Garrison et al., 2015) with fMRI and Civier and colleagues (2019) (Civier et al., 2019) with DTI, showing that in EEG studies the thresholding should be used with considerable caution. Our study shows that the networks on the different thresholds are obscured by the global measures, as similar values of global measures could be estimated from the variety of structurally different networks. Most importantly, the network structure estimated for the different thresholds may lead to different conclusions of a study. The basic idea of the thresholding procedure (clearing the weak edges out) implies that detecting a stable experimental effect is only possible in the absence of spurious connections (at high thresholds). Our results indicate that the presence of an effect can also be detected at significantly lower threshold levels and its direction can even be the opposite if the weak connections are preserved. This requires a more thoughtful and informed approach to the thresholding procedure.

One of the main challenges in the functional connectivity thresholding problem stems from the fact that there is by now no “ground truth” method on how to define the best threshold value. While the structure-function relationships are an essential part of complex natural systems, it seems that the link between structural connections and functional connectivity can be fundamentally imperfect. Even though the architecture of the structural connectivity networks shapes the boundaries of the functional network, the actual neural dynamics may not be perfectly aligned to it (Suárez et al., 2020). However, it is still important to provide a basis

under the used threshold level. Recently, an approach to choose the thresholding value according to the entropy of the functional networks has been suggested (Nicolini et al., 2020), however, its validity and reliability are yet to be established.

The data-driven approach based on the MST algorithms has been proposed as a solution to the problem of choosing the arbitrary threshold for network construction (Dimitriadis et al., 2017). The MST is supposed to reduce the influence of the spurious connections within the brain by considering strong connections within the brain that don't form cycles or loops thus achieving higher specificity of network topological properties. However, several studies have shown that weak connections can play a significant role when investigating the links between network properties and individual differences in behaviour. The importance of weak connections for network stability has been established for various complex systems, from protein-to-protein interaction (Ma & Gao, 2012), to mobile communication networks (Onnela et al., 2007), biological functions (Csermely, 2004) or social networks (Granovetter, 1983). According to the recent anatomical studies with tracing the connections within the cortical, the brain indeed has a lot of weak connections that has a substantial impact on maintaining the intermodular connections between functional brain modules. Weak connections may also play a significant role in the individual differences in intelligence (Santarnecchi et al., 2014; Zakharov et al., 2020) and its abnormality may be related to the symptomatology of schizophrenic patients (Bassett et al., 2012).

One way to overcome the existing thresholding-related problems with network analysis may be to widen the description of the networks with local (nodal) measures and to describe the network more thoroughly with a set of different measures, such as graphlets. Graphlet can be defined as an induced subgraph isomorphism class in a graph. Graphlets have been suggested for the analysis of the topological structure of the undirected networks (Yaveroğlu et al., 2014), which is important for brain functional connectivity analysis, where networks are mainly undirected by construction.

The variability in the graph-metrics estimation related to thresholding procedure is just a part of a bigger problem of the variability in the analysis pipelines in neuroimaging data. Recently, the results from 70 research teams focused on analyzing the same datasets showed that the analytic choices, made by researchers, lead to the substantial affect variability in the research conclusions (Botvinik-Nezer et al., 2020). To directly estimate the role of such variability in the EEG research the open EEG Many Pipelines has been launched (https://www.eegmanypipelines.org/).

Is there anything that can be done to choose among the vast amount of possible analytic choices? In our opinion, there are several possible answers. One solution may lie in data sharing, that opens the possibility to test whether different analysis will lead to the comparable results (for the discussion regarding open data practices see Munafò et al., 2017)). Another way to overcome the huge variability in the data analysis is the pre-registration practices (Hardwicke & Ioannidis, 2018). The idea of pre-registration is to have a record (public or stored in the journal editorial office) of the detailed analysis plan prior to the data collection. Current experience shows that pre-registration leads to higher level of the replicability of the research

(Soderberg et al., 2021). Finally, analysis of complex datasets can be performed according to the multiverse approach (Steegen et al., 2016). According to the multiverse approach the overall conclusion regarding the effects of interest can rely only on comparing various analysis procedures (Harder, 2020). To additionally increase the integrity and the reproducibility of these analyses the analysts can also be "blinded" regarding the initial hypothesis of the research. Recently, the guideline for multi-analyst research emerged (Aczel et al., 2021) wrapping up the techniques of strengthening the robustness of scientific results. As the different analysis pipelines used by research groups could possibly lead to different conclusions, authors encourage independent researchers to perform an analysis on the same data, inferring the robust result where results from the different researchers converge.

To sum up, in the present study we have shown that in agreement with the broader problem of the analytic choices in neuroimaging studies, the analysis of the brain connectivity can be highly dependent on choosing the thresholds for connectivity matrix construction with no best way to choose between different analytic options. Different approaches, such as multiverse analysis or analysis by different research teams are advocated for.

Methods

Participants

164 participants, aged from 17 to 34 years (M=21.7, SD = 3.36, 30% female) with no report of head traumas or psychiatric or neurological disorders took part in our study. Each participant gave an informed consent to participate in the study. No monetary reward was given to the participants. The study was approved by the ethical committee of the Psychological Institute of Russian Academy of Education.

Experimental procedure and data acquisition

Brain Products ActiChamp was used for the 64-channel EEG recording with a 500Hz sampling rate. Cz electrode was used as a reference. EEG preprocessing included four steps: 1) Downsampling to 256Hz, 2) Re-reference to a common reference, 3) Filtering from 1Hz to 30Hz and 4) artefact removal. An artefact removal consisted of manual removal of artefacts, removal of ocular artifacts via an infomax Independent Component Analysis and topographic interpolation of the noisy channels.

The experimental procedure consists of five alternating 2-minute intervals with closed and open eyes. Total 10 minutes per participant were recorded with 3 closed-eyes intervals. Only closed-eyes condition was used in the study.

Source reconstruction

Source reconstruction was performed using the pipeline mentioned in the documentation to the MNE package (Gramfort et al., 2014). The source reconstruction was performed based on a three-layer BEM model with 1026 sources per hemisphere. The three layers represent the inner skull, outer skull and outer skin and the conductivity of the layers was standard for the MNE package (0.3, 0.006 and 0.3). To construct the BEM model, the standard FreeSurfer model head, Colin27, was used. The individual source reconstruction was performed with the individual inverse operator using the dSPM method. Cortical parcellation was achieved via the MNE function mne.extract_label_time_course with "pca_flip" method with the Desikan-Killiany Atlas (Desikan et al., 2006).

Estimation of synchronization

Five measures were used to estimate synchronization: weighted phase lag index (wPLI, Vinck et al., 2011), Imaginary part of Coherency (imcoh, Nolte et al., 2004), coherence, corrected imaginary phase locking value (ciPLV, Bruña et al., 2018) and the Pairwise Phase Consistency (PPC, Vinck et al., 2010). Each of these measures has their own assumptions and are easily available via common EEG-analysis packages (e.g. MNE for Python). Synchronization was estimated in alpha band 8-13 Hz frequency range for sensor and source space with each synchronization measure for eyes-closed condition.

Graph analysis

The NetworkX package (Hagberg et al., 2008) was used for the graph analysis. Each connectivity matrix was considered as a weighted graph adjacency matrix. Threshold values started from 0.01 quantile of the matrix weights distribution (99% of the connections included) to 0.99 (1% of the strongest connections included) with 0.01 step. Edges with weight below the threshold were eliminated. On each step, disconnected nodes were removed and are reported as isolated nodes. In case the graph divides into separate subgraphs only the biggest component remains. The graph structure on each threshold was constructed based on the probability of edge existence in the whole sample. The probability of edge existence for each edge was defined as the ratio of adjacency matrices with non-zero edge weight to the total number of adjacency matrices. The probability graphs were constructed for each threshold.

Another way to construct the graph is based on the minimum spanning tree (MST) algorithms. The minimum spanning tree is a set of edges that connects all nodes with minimum possible edge weight. We use the orthogonal MST algorithm developed by G. Dimitriadis (Dimitriadis et al., 2017). The orthogonal MST method implies the consequent extraction of MSTs from the full graph. The MST on each step is removed from the original graph (all edges belonging to the MST are set to zero), but it is transferred to a new, thresholded network. The algorithm ends when an equilibrium between global efficiency and edge removal cost is

reached. We compare the data-driven graphs with the same density traditionally thresholded graph.

For each graph, we calculated four measures to describe the network structure: Characteristic Path Length, Clustering Coefficient, participation coefficient and SWI.

The Characteristic path length is defined as the median of the distribution number of edges between two nodes in the shortest distance between them.

The clustering coefficient is a measure of the tendency of nodes to form interconnected groups. For each node clustering coefficient is a proportion of the existing number of connections in a neighbourhood to a total number of possible connections.

Participation coefficient is a measure of node edge distribution across networks calculated for each node. Nodes with uniform link distribution with other nodes will have participation coefficient 1, if a node has edges among one specific community, the participation coefficient will be 0. The mean participation centrality across all nodes is presented.

SWI (Small-world Index, Humphries et al., 2006) is a measure of a small-worldness of the graph via the comparison of the characteristic path length and clustering coefficient of a given graph with the measures in the set of random graphs.

Statistical analysis

Linear regression analysis was performed to estimate the graph measure dynamic. A permutation t-test was used to estimate the differences between traditional and data-driven approaches and group differences. Spearman correlation coefficient was used for estimation of the similarity between different thresholds. The connectivity matrices were created via the MNE package (Gramfort et al., 2013, 2014), graph analysis was performed in NetworkX (Hagberg et al., 2008), OMST-graphs were created via authors package in Matlab (https://github.com/stdimitr/multi-group-analysis-OMST-GDD), statistical analysis was performed in R in stats (https://www.r-project.org/) and exactRankTests (https://CRAN.R-project.org/package=exactRankTests) packages

References

Aczel, B., Szaszi, B., Nilsonne, G., van den Akker, O. R., Albers, C. J., van Assen, M. A., Bastiaansen, J. A., Benjamin, D., Boehm, U., Botvinik-Nezer, R., Bringmann, L. F., Busch, N. A., Caruyer, E., Cataldo, A. M., Cowan, N., Delios, A., van Dongen, N. N., Donkin, C., van Doorn, J. B., … Wagenmakers, E.-J. (2021). Consensus-based guidance for conducting and reporting multi-analyst studies. *ELife*, *10*, e72185. https://doi.org/10.7554/eLife.72185

Allen, E. A., Damaraju, E., Eichele, T., Wu, L., & Calhoun, V. D. (2018). EEG Signatures of Dynamic Functional Network Connectivity States. *Brain Topography*, *31*(1), 101–116. https://doi.org/10.1007/s10548-017-0546-2

Avena-Koenigsberger, A., Misic, B., & Sporns, O. (2018). Communication dynamics in complex brain networks. *Nature Reviews Neuroscience*, *19*(1), 17–33. https://doi.org/10.1038/nrn.2017.149

Babiloni, C., Barry, R. J., Başar, E., Blinowska, K. J., Cichocki, A., Drinkenburg, W. H. I. M., Klimesch, W., Knight, R. T., Lopes da Silva, F., Nunez, P., Oostenveld, R., Jeong, J., Pascual-Marqui, R., Valdes-Sosa, P., & Hallett, M. (2020). International Federation of Clinical Neurophysiology (IFCN) – EEG research workgroup: Recommendations on frequency and topographic analysis of resting state EEG rhythms. Part 1: Applications in clinical research studies. *Clinical Neurophysiology*, *131*(1), 285–307. https://doi.org/10.1016/j.clinph.2019.06.234

Bassett, D. S., Nelson, B. G., Mueller, B. A., Camchong, J., & Lim, K. O. (2012). Altered Resting State Complexity in Schizophrenia. *Neuroimage*, *59*(3), 2196–2207. https://doi.org/10.1016/j.neuroimage.2011.10.002

Bastos, A. M., & Schoffelen, J.-M. (2016). A Tutorial Review of Functional Connectivity Analysis Methods and Their Interpretational Pitfalls. *Frontiers in Systems Neuroscience*, *9*. https://doi.org/10.3389/fnsys.2015.00175

Bastos, A. M., Vezoli, J., & Fries, P. (2015). Communication through coherence with inter-areal delays. *Current Opinion in Neurobiology*, *31*, 173–180. https://doi.org/10.1016/j.conb.2014.11.001

Beaty, R. E., Kenett, Y. N., Christensen, A. P., Rosenberg, M. D., Benedek, M., Chen, Q., Fink, A., Qiu, J., Kwapil, T. R., Kane, M. J., & Silvia, P. J. (2018). Robust prediction of individual creative ability from brain functional connectivity. *Proceedings of the National Academy of Sciences*, *115*(5), 1087–1092. https://doi.org/10.1073/pnas.1713532115

Botvinik-Nezer, R., Holzmeister, F., Camerer, C. F., Dreber, A., Huber, J., Johannesson, M., Kirchler, M., Iwanir, R., Mumford, J. A., Adcock, R. A., Avesani, P., Baczkowski, B. M., Bajracharya, A., Bakst, L., Ball, S., Barilari, M., Bault, N., Beaton, D., Beitner, J., … Schonberg, T. (2020). Variability in the analysis of a single neuroimaging dataset by many teams. *Nature*, *582*(7810), 84–88. https://doi.org/10.1038/s41586-020-2314-9

Bruña, R., Maestú, F., & Pereda, E. (2018). *Phase locking value revisited: Teaching new tricks to an old dog*. *15*(5), 056011. https://doi.org/10.1088/1741-2552/aacfe4

Buchanan, C. R., Bastin, M. E., Ritchie, S. J., Liewald, D. C., Madole, J. W., Tucker-Drob, E. M., Deary, I. J., & Cox, S. R. (2020). The effect of network thresholding and weighting on structural brain networks in the UK Biobank. *NeuroImage*, *211*, 116443. https://doi.org/10.1016/j.neuroimage.2019.116443

Buckner, R. L., Krienen, F. M., & Yeo, B. T. T. (2013). Opportunities and limitations of intrinsic functional connectivity MRI. *Nature Neuroscience*, *16*(7), 832–837. https://doi.org/10.1038/nn.3423

Civier, O., Smith, R. E., Yeh, C.-H., Connelly, A., & Calamante, F. (2019). Is removal of weak connections necessary for graph-theoretical analysis of dense weighted structural connectomes from diffusion MRI? *NeuroImage*, *194*, 68–81. https://doi.org/10.1016/j.neuroimage.2019.02.039

Csermely, D. (2004). Lateralisation in birds of prey: Adaptive and phylogenetic considerations. *Behavioural Processes*, *67*(3), 511–520. https://doi.org/10.1016/j.beproc.2004.08.008

Desikan, R. S., Ségonne, F., Fischl, B., Quinn, B. T., Dickerson, B. C., Blacker, D., Buckner, R. L., Dale, A. M., Maguire, R. P., Hyman, B. T., Albert, M. S., & Killiany, R. J. (2006). An automated labeling system for subdividing the human cerebral cortex on MRI scans into gyral based regions of interest. *NeuroImage*, *31*(3), 968–980. https://doi.org/10.1016/j.neuroimage.2006.01.021

Dimitriadis, S. I., López, M. E., Bruña, R., Cuesta, P., Marcos, A., Maestú, F., & Pereda, E. (2018). How to Build a Functional Connectomic Biomarker for Mild Cognitive Impairment From Source Reconstructed MEG Resting-State Activity: The Combination of ROI Representation and Connectivity Estimator Matters. *Frontiers in Neuroscience*, *12*. https://doi.org/10.3389/fnins.2018.00306

Dimitriadis, S. I., Routley, B., Linden, D. E., & Singh, K. D. (2018). Reliability of Static and Dynamic Network Metrics in the Resting-State: A MEG-Beamformed Connectivity Analysis. *Frontiers in Neuroscience*, *12*, 506. https://doi.org/10.3389/fnins.2018.00506

Dimitriadis, S. I., Salis, C., Tarnanas, I., & Linden, D. E. (2017). Topological Filtering of Dynamic Functional Brain Networks Unfolds Informative Chronnectomics: A Novel Data-Driven Thresholding Scheme Based on Orthogonal Minimal Spanning Trees (OMSTs). *Frontiers in Neuroinformatics*, *11*. https://doi.org/10.3389/fninf.2017.00028

Finn, E. S., Shen, X., Scheinost, D., Rosenberg, M. D., Huang, J., Chun, M. M., Papademetris, X., & Constable, R. T. (2015). Functional connectome fingerprinting: Identifying individuals based on patterns of brain connectivity. *Nature Neuroscience*, *18*(11), 1664–1671. https://doi.org/10.1038/nn.4135

Fries, P. (2015). Rhythms For Cognition: Communication Through Coherence. *Neuron*, *88*(1), 220–235. https://doi.org/10.1016/j.neuron.2015.09.034

Garrison, K. A., Scheinost, D., Finn, E. S., Shen, X., & Constable, R. T. (2015). The (in)stability of functional brain network measures across thresholds. *NeuroImage*, *118*, 651–661. https://doi.org/10.1016/j.neuroimage.2015.05.046

Gramfort, A., Luessi, M., Larson, E., Engemann, D. A., Strohmeier, D., Brodbeck, C., Parkkonen, L., & Hämäläinen, M. S. (2014). MNE software for processing MEG and EEG data. *NeuroImage*, *86*, 446–460. https://doi.org/10.1016/j.neuroimage.2013.10.027

Gramfort, A., Luessi, M., Larson, E., Engemann, D., Strohmeier, D., Brodbeck, C., Goj, R., Jas, M., Brooks, T., Parkkonen, L., & Hämäläinen, M. (2013). MEG and EEG data analysis with MNE-Python. *Frontiers in Neuroscience*, *7*, 267. https://doi.org/10.3389/fnins.2013.00267

Granovetter, M. (1983). The Strength of Weak Ties: A Network Theory Revisited. *Sociological Theory*, *1*, 201–233. JSTOR. https://doi.org/10.2307/202051

Hagberg, A. A., Schult, D. A., & Swart, P. J. (2008). *Exploring Network Structure, Dynamics, and Function using NetworkX*. 5.

Harder, J. A. (2020). The Multiverse of Methods: Extending the Multiverse Analysis to Address Data-Collection Decisions. *Perspectives on Psychological Science*, *15*(5), 1158–1177. https://doi.org/10.1177/1745691620917678

Hardwicke, T. E., & Ioannidis, J. P. A. (2018). Mapping the universe of registered reports. *Nature Human Behaviour*, *2*(11), 793–796. https://doi.org/10.1038/s41562-018-0444-y

Humphries, M. D., Gurney, K., & Prescott, T. J. (2006). The brainstem reticular formation is a small-world, not scale-free, network. *Proceedings of the Royal Society B: Biological Sciences*, *273*(1585), 503–511. https://doi.org/10.1098/rspb.2005.3354

Liégeois, R., Laumann, T. O., Snyder, A. Z., Zhou, J., & Yeo, B. T. T. (2017). Interpreting temporal fluctuations in resting-state functional connectivity MRI. *NeuroImage*, *163*, 437–455. https://doi.org/10.1016/j.neuroimage.2017.09.012

Ma, X., & Gao, L. (2012). Discovering protein complexes in protein interaction networks via exploring the weak ties effect. *BMC Systems Biology*, *6 Suppl 1*, S6. https://doi.org/10.1186/1752-0509-6-S1-S6

Markett, S., Montag, C., & Reuter, M. (2018). Network Neuroscience and Personality. *Personality Neuroscience*, *1*. https://doi.org/10.1017/pen.2018.12

Munafò, M. R., Nosek, B. A., Bishop, D. V. M., Button, K. S., Chambers, C. D., Percie du Sert, N., Simonsohn, U., Wagenmakers, E.-J., Ware, J. J., & Ioannidis, J. P. A. (2017). A manifesto for reproducible science. *Nature Human Behaviour*, *1*(1), 1–9. https://doi.org/10.1038/s41562-016-0021

Nicolini, C., Forcellini, G., Minati, L., & Bifone, A. (2020). Scale-resolved analysis of brain functional connectivity networks with spectral entropy. *NeuroImage*, *211*, 116603. https://doi.org/10.1016/j.neuroimage.2020.116603

Nolte, G., Bai, O., Wheaton, L., Mari, Z., Vorbach, S., & Hallett, M. (2004). Identifying true brain interaction from EEG data using the imaginary part of coherency. *Clinical Neurophysiology*, *115*(10), 2292–2307. https://doi.org/10.1016/j.clinph.2004.04.029

Onnela, J.-P., Saramäki, J., Hyvönen, J., Szabó, G., Lazer, D., Kaski, K., Kertész, J., & Barabási, A.-L. (2007). Structure and tie strengths in mobile communication networks. *Proceedings of the National Academy of Sciences*, *104*(18), 7332–7336. https://doi.org/10.1073/pnas.0610245104

Palva, S., & Palva, J. M. (2011). Functional Roles of Alpha-Band Phase Synchronization in Local and Large-Scale Cortical Networks. *Frontiers in Psychology*, *2*, 204. https://doi.org/10.3389/fpsyg.2011.00204

Rubinov, M., & Sporns, O. (2010). Complex network measures of brain connectivity: Uses and interpretations. *NeuroImage*, *52*(3), 1059–1069. https://doi.org/10.1016/j.neuroimage.2009.10.003

Sadaghiani, S., Brookes, M. J., & Baillet, S. (2022). Connectomics of human electrophysiology. *NeuroImage*, *247*, 118788. https://doi.org/10.1016/j.neuroimage.2021.118788

Santarnecchi, E., Galli, G., Polizzotto, N. R., Rossi, A., & Rossi, S. (2014). Efficiency of weak brain connections support general cognitive functioning. *Human Brain Mapping*, *35*(9), 4566–4582. https://doi.org/10.1002/hbm.22495

Smith, R. X., Jann, K., Dapretto, M., & Wang, D. J. J. (2018). Imbalance of Functional Connectivity and Temporal Entropy in Resting-State Networks in Autism Spectrum Disorder: A Machine Learning Approach. *Frontiers in Neuroscience*, *12*. https://doi.org/10.3389/fnins.2018.00869

Soderberg, C. K., Errington, T. M., Schiavone, S. R., Bottesini, J., Thorn, F. S., Vazire, S., Esterling, K. M., & Nosek, B. A. (2021). Initial evidence of research quality of registered reports compared with the standard publishing model. *Nature Human Behaviour*, *5*(8), 990–997. https://doi.org/10.1038/s41562-021-01142-4

Stam, C. J., & van Straaten, E. C. W. (2012). The organization of physiological brain networks. *Clinical Neurophysiology*, *123*(6), 1067–1087. https://doi.org/10.1016/j.clinph.2012.01.011

Steegen, S., Tuerlinckx, F., Gelman, A., & Vanpaemel, W. (2016). Increasing Transparency Through a Multiverse Analysis. *Perspectives on Psychological Science*, *11*(5), 702–712. https://doi.org/10.1177/1745691616658637

Stevens, W. D., & Spreng, R. N. (2014). Resting-state functional connectivity MRI reveals active processes central to cognition. *WIREs Cognitive Science*, *5*(2), 233–245. https://doi.org/10.1002/wcs.1275

Suárez, L. E., Markello, R. D., Betzel, R. F., & Misic, B. (2020). Linking Structure and Function in Macroscale Brain Networks. *Trends in Cognitive Sciences*, *24*(4), 302–315. https://doi.org/10.1016/j.tics.2020.01.008

Toschi, N., Riccelli, R., Indovina, I., Terracciano, A., & Passamonti, L. (2018). Functional Connectome of the Five-Factor Model of Personality. *Personality Neuroscience*, *1*. https://doi.org/10.1017/pen.2017.2

van den Heuvel, M. P., & Sporns, O. (2019). A cross-disorder connectome landscape of brain dysconnectivity. *Nature Reviews. Neuroscience*, *20*(7), 435–446. https://doi.org/10.1038/s41583-019-0177-6

van Diessen, E., Numan, T., van Dellen, E., van der Kooi, A. W., Boersma, M., Hofman, D., van Lutterveld, R., van Dijk, B. W., van Straaten, E. C. W., Hillebrand, A., & Stam, C. J. (2015). Opportunities and methodological challenges in EEG and MEG resting state functional brain network research. *Clinical Neurophysiology*, *126*(8), 1468–1481. https://doi.org/10.1016/j.clinph.2014.11.018

van Wijk, B. C. M., Stam, C. J., & Daffertshofer, A. (2010). Comparing Brain Networks of Different Size and Connectivity Density Using Graph Theory. *PLoS ONE*, *5*(10), e13701. https://doi.org/10.1371/journal.pone.0013701

Vinck, M., Oostenveld, R., van Wingerden, M., Battaglia, F., & Pennartz, C. M. A. (2011). An improved index of phase-synchronization for electrophysiological data in the presence of volume-conduction, noise and sample-size bias. *NeuroImage*, *55*(4), 1548–1565. https://doi.org/10.1016/j.neuroimage.2011.01.055

Vinck, M., van Wingerden, M., Womelsdorf, T., Fries, P., & Pennartz, C. M. A. (2010). The pairwise phase consistency: A bias-free measure of rhythmic neuronal synchronization. *NeuroImage*, *51*(1), 112–122. https://doi.org/10.1016/j.neuroimage.2010.01.073

Yaveroğlu, Ö. N., Malod-Dognin, N., Davis, D., Levnajic, Z., Janjic, V., Karapandza, R., Stojmirovic, A., & Pržulj, N. (2014). Revealing the Hidden Language of Complex Networks. *Scientific Reports*, *4*(1), 4547. https://doi.org/10.1038/srep04547

Zakharov, I., Adamovich, T., Tabueva, A., Ismatullina, V., & Malykh, S. (2021). The effect of density thresholding on the EEG network construction. *Journal of Physics: Conference Series*, *1727*, 012009. https://doi.org/10.1088/1742-6596/1727/1/012009

Zakharov, I., Tabueva, A., Adamovich, T., Kovas, Y., & Malykh, S. (2020). Alpha Band Resting-State EEG Connectivity Is Associated With Non-verbal Intelligence. *Frontiers in Human Neuroscience*, *14*. https://doi.org/10.3389/fnhum.2020.00010

Appendix

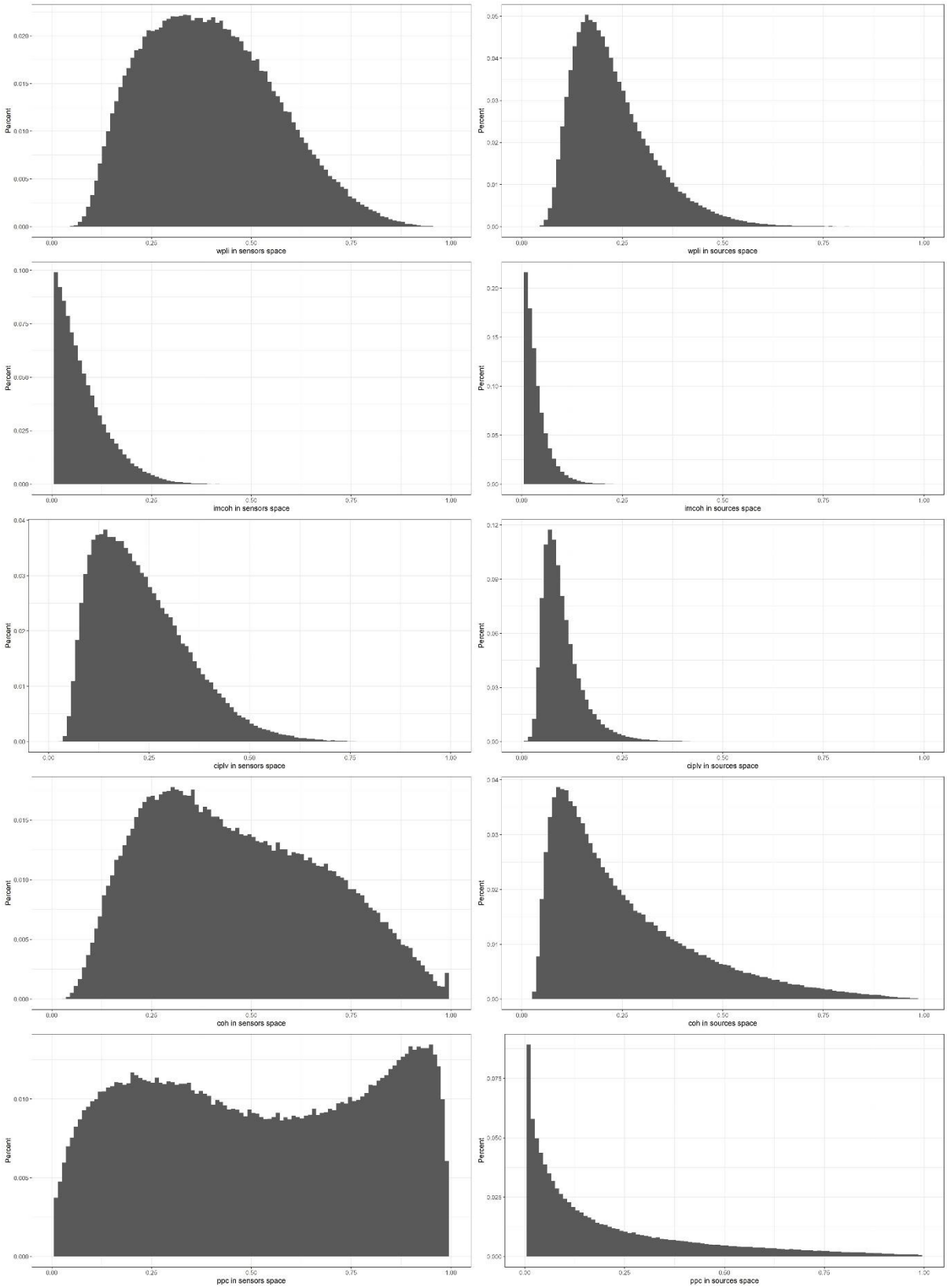

Figure 1. Distributions of synchronization measures

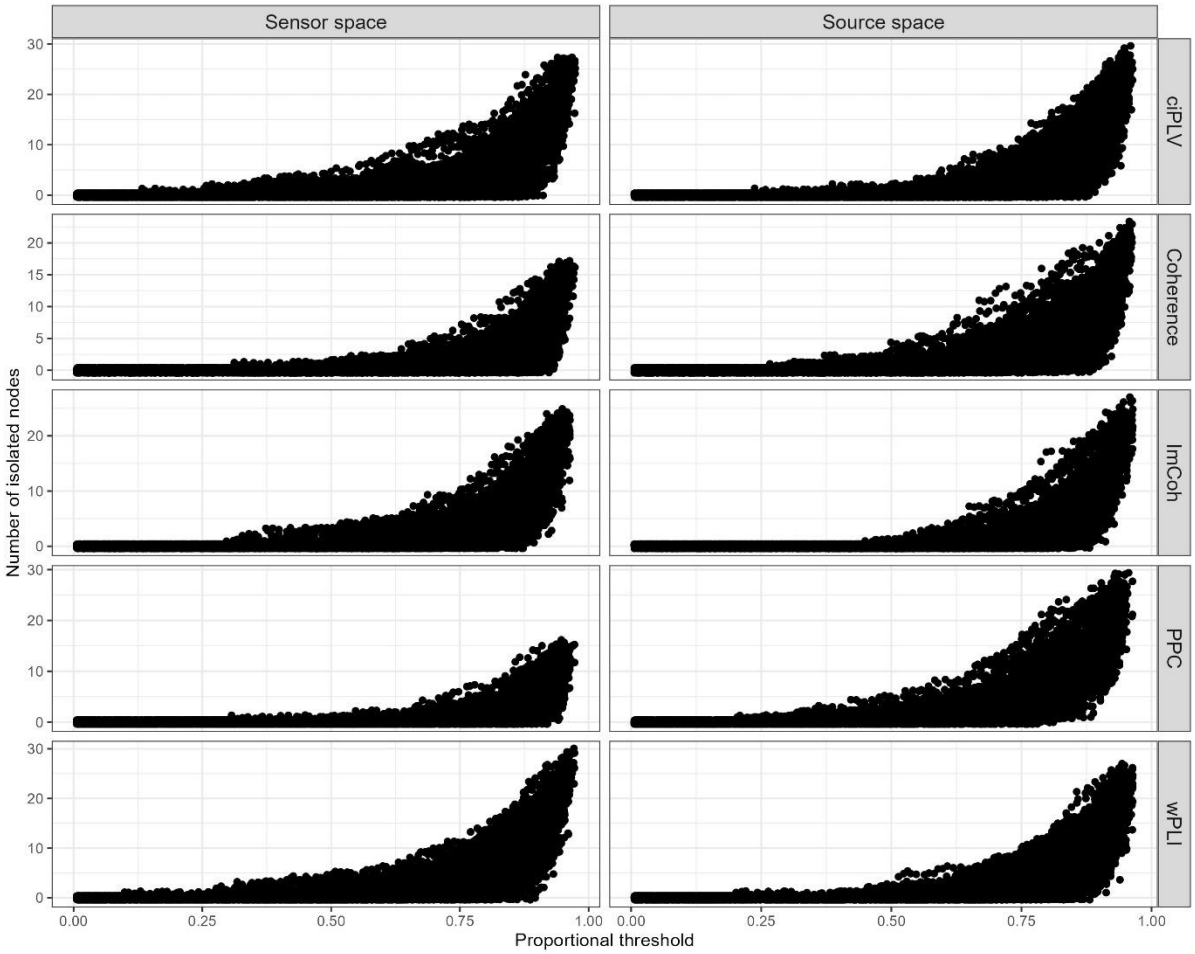

Figure 2. A number of isolated nodes across different thresholds. Each node represents one matrix.

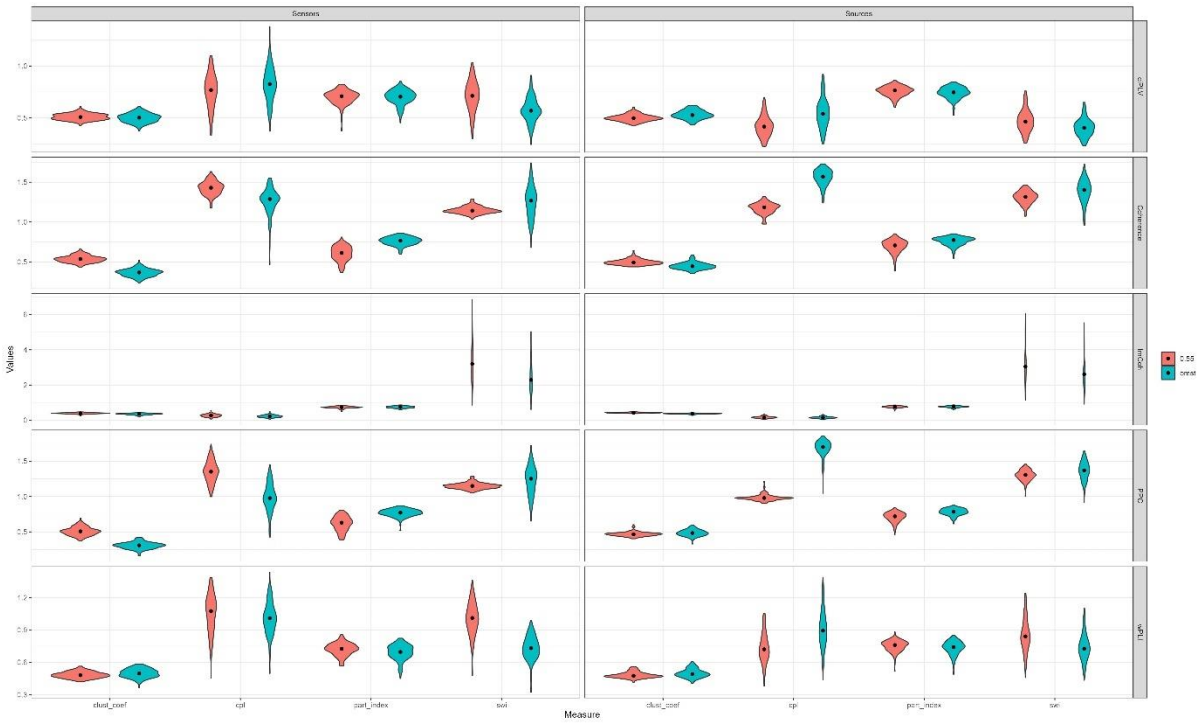

Picture 3. Comparison of the measures derived from the thresholded graph (red) and OMST-graph (blue).